Modeling Side-Stream Enhanced Biological Phosphorus Removal (S2EBPR) System Using Agent-based Model with Adaptive Maintenance, Decay and TCA Metabolism

Guangyu Li [1], Nicholas B. Tooker [1], Dongqi Wang [1,2], Varun Srinivasan [1], James L. Barnard [3], Andrew Russell [4], Imre Takacs [5], Charles Bott [6], Paul Dobrowski [7], Annalisa Onnis-Hayden [1], and April Z. Gu [8,*]

[1] Department of Civil & Environmental Engineering, Northeastern University, Boston, MA, United States

[2] Department of Municipal and Environmental Engineering, Xi'an University of Technology, Xi'an, Shaanxi, China

[3] Black & Veatch, Kansas City, MO, United States

[4] South Cary Water Reclamation Facility, Apex, NC, United States

[5] Dynamita, Nyons, France

[6] Hampton Roads Sanitation District, Virginia Beach, VA, 23454, United States

[7] Woodard & Curran, Inc., CT, 06082, United States

[8] School of Civil and Environmental Engineering, Cornell University, Ithaca, NY, United States

KEYWORDS: EBPR, S2EBPR, Agent-based modeling, Cell maintenance, Cell decay, Glycolysis-TCA pathway switch

ABSTRACT

Side-stream enhanced biological phosphorus removal process (S2EBPR) refers to modified EBPR configurations that have been demonstrated to improve the performance stability and offer a suite of advantages compared to conventional EBPR design. Design and optimization of S2EBPR requires modification of the current EBPR models that were not able to fully reflect the metabolic functions of and competition between the PAOs and GAOs under extended anaerobic conditions as in the S2EBPR conditions. In this study, we proposed and validated an improved iEBPR model for simulating PAO and GAO competition that incorporated heterogeneity and versatility in PAO sequential polymer usage, staged maintenance-decay and glycolysis-TCA pathway shifts. The iEBPR model was first calibrated against a bulk batch test experimental data. The improved iEBPR model performed better than the previous EBPR model for predicting the soluble orthoP, ammonia, biomass glycogen and PHA temporal profiles in a batch starvation testing under prolong anaerobic conditions. We further validated the model with another independent set of batch anaerobic batch testing data that included high-resolution cellular and population-level intracellular polymers measurements enabled by single-cell Raman microspectroscopy technique. The model accurately predicted the temporal changes in the intracellular polymers at cellular and population levels within PAOs and GAOs, further confirmed the proposed mechanism of sequential polymer utilization, and polymer availability-dependent and staged maintenance and decay in PAOs. These results indicate that under extended anaerobic phases as in S2EBPR, the PAOs may gain competitive advantage over GAOs due to the possession of multiple intracellular polymers and the adaptive switching of the anaerobic metabolic pathways that consequently lead to the later and slower decay in PAOs than GAOs. The iEBPR model can be applied to facilitate and optimize the

design and operations of S2EBPR for more reliable nutrient removal and recovery from wastewater.

INTRODUCTION

Enhanced biological phosphorus removal (EBPR) process has been recommended as a promising strategy to achieve sustainable wastewater P removal and simultaneous P recovery [1]. Current EBPR systems are driven by and engineered to favor a key functional group, phosphate-accumulating organisms (PAOs) such as the *Candidatus Accumulibacter phosphatis*, which is the most commonly found PAO in EBPR systems. Glycogen-accumulating organisms (GAOs) are often found to coexist with PAOs but lacking polyP metabolism. They have similar glycogen-based VFA-PHA metabolism [2,3] concerned to be niche VFA competitor with PAOs but have limited contribution to P removal performance. PAO-GAO competition could be a critical factor in EBPR performance and is kinetically affected by various factors including pH, temperature and hydraulic retention time (HRT) etc. [4–8]. Meanwhile, the existence of GAOs does not necessarily deteriorate EBPR performance as long as PAOs are kinetically favored [1,9,10].

The performance stability of EBPR has been a concern for its wide implementation in practice and its sustainability advantages are often offset by the needs to have chemicals standby for ensuring reliable P removal performance to consistently meet compliance [1,9,11]. Many facilities still suffer from inconsistent performance with unpredicted upsets, particularly for those with relatively weak influent readily biodegradable COD (rbCOD) [1,5,6,12]. An emerging technology that has been demonstrated to successfully address this common stability challenge is side-stream RAS and mixed liquor hydrolysis/fermentation-based side-stream EBPR (S2EBPR) [1,9,11,13–18]. S2EBPR refers to modified EBPR configurations that include diversion of a portion of RAS or anaerobic

66 mixed liquor to a side-stream reactor, where simultaneous VFA production via sludge hydrolysis
67 and fermentation and PAO activity-related P release and carbon uptake occur. Compared to
68 conventional EBPR design, the S2EBPR offers a suite of advantages including influent-carbon
69 independent condition for PAO enrichment that eliminates the influences of fluctuating influent
70 loads, more controllable lower-redox environment with more complex VFA composition that
71 provides more favorable selection of PAOs over GAOs, flexible implementation configurations
72 and potential reduction of carbon footprint and denitrification enhancement by diverting more
73 influent carbon to denitrification [1,9,11,19–22]..

74 While full-scale processes demonstrated the potential promises and advantages of S2EBPR [9,11,13–
75 18], existing knowledge gaps in fundamental understanding of the biochemical mechanisms and
76 microbial ecology involved in S2EBPR hampers its wider application and implementation. Design
77 and optimization of S2EBPR requires adequate EBPR models that can capture the underlying key
78 mechanisms involved in the S2EBPR such as the VFA production via hydrolysis and fermentation,
79 and PAO and GAO competition in the extended-anaerobic side-stream reactor. A few recent
80 modeling efforts failed to predict either this competitive advantage or the performance superiority
81 observed in S2EBPR systems compared to the conventional EBPR systems [23,24]. This suggested
82 that there are still critical aspects in the current EBPR models that cannot reflect the metabolic
83 functions of and competition between the PAOs and GAOs under the S2EBPR conditions, such as
84 cell maintenance, biomass decay, the utilization of intracellular polymers, and PAO/GAO
85 metabolic versatility under the prolonged anaerobic condition [25,26].

86 PAOs' cell maintenance is a hypothesized metabolic process from the observation of their steady-
87 state and consistent intracellular glycogen and polyP degradation that are independent of their

EBPR-related metabolic activities such as PHA synthesis [2,4,24,27–31]. Studies showed that PAOs continued consuming their intracellular glycogen and polyP both during short-term (about 10 hrs) [4,27,28] and long-term (≥5 days) [29] anaerobic treatments without external VFA supply and they were not coupled with EBPR-associated VFA uptake and storage. Similar experimental evidence was observed for GAOs who had cell maintenance during both short-term [2,24,30,31] and long-term [29] anaerobic conditions solely based on glycogen. The possession and ability to utilize both polyP and glycogen depending on their availability for maintenance energy derivation by PAOs led to the seemingly inconsistent observations of polymer utilization priority under the similar anaerobic conditions. This highlighted the importance of the more pronounced effects of anaerobic metabolic versatility of PAOs, particularly under extended anaerobic condition such as those in S2EBPRs [32,33]. However, in current EBPR models, PAO cell maintenance is often approximated by either first-order decay of polyP and/or glycogen (e.g. ASM2 and ASM3+BioP [34]), or polyP-only cleavage (e.g. Barker&Dold and UCTPHO+ [35,36]) without accounting for glycogen. Recent studies attempted sequential polymer usage strategy [26,37,38] to mitigate the overestimation of polymer consumption encountered in traditional EBPR models that use first-order decay (e.g. ASM2 and ASM3+BioP [34]) and polyP cleavage (e.g. Barker&Dold and UCTPHO+ [35,36], which ignores glycogen). More accurate modeling of the cell maintenance processes in PAOs and GAOs under the unique and prolonged anaerobic conditions can improve the modeling efficiency of S2EBPR systems[39]. Li et al. (2018; 2020) and Santos et al. (2020) further extended the cell maintenance to the "survival" hypothesis, in which maintenance precedes biomass decay, to explain the observed low PAO/GAO decay rate in comparison to other heterotrophic organisms under anaerobic conditions [26,38,40]. However, with complex microbial communities, current population-level

models still cannot estimate the effect of mixture phenotypes and non-uniformity in polymer distributions [8,41] and capture the detailed PAO-GAO competition at phenotype/cell group level.

The most debated aspect related to the Accumulibacter's anaerobic metabolism is the source of reducing power (NAD(P)H). In early studies, this source was deduced to be exclusively supported by glycolysis (referred to as Mino model) [42] or solely supported by tricarboxylic acid (TCA) cycle (referred to as Comeau-Wentzel model) [27,43]. Both models were supported by additional experiments [4,44], while some others suggested potential coexistence and simultaneous contribution to t NAD(P)H production [45–48]. A switch between these pathways may occur and was hypothesized to be related with intracellular polymer availability or depletion [25,45,48,49]. Another critical discussion on the anaerobic operation of complete TCA proposed that the oxidation of succinate thermodynamically is unfavorable which relies on external electron acceptors (TEAs) [28]. Four potential mechanisms have been proposed that either bypass this oxidation step or employ alternative ways to sink the electrons, namely succinate-propionate shunt [50], partial reductive TCA cycle [50–52], glyoxylate shunt [47,53,54] or proton motive force-driven quinol-NAD(P)$^+$ reductase [55]. Each proposed theoretical pathway was supported by physiological, genomics, transcriptomics or proteomics evidences, and exhibits different stoichiometry on glycogen, polyP, VFAs, PHAs and CO_2 release. This metabolic versatility may help explain the wide range of stoichiometry observed in a variety of full-scale studies [25]. Santos et al. (2020) introduced the pathway switching mechanism to better reproduce this complicated, flexible metabolic network [38]. However, traditional EBPR models cannot simulate such pathway shift effects as the essential yield coefficients was kept constant during the simulation after calibration, nor distinguish between coexisting PAO phenotypes with different glycolysis and TCA cycle operations.

In this study, with the long-term goal to better predict the S2EBPR processes, we proposed and validated an improved model for PAO and GAO competition under extended anaerobic conditions that incorporated heterogeneity and versatility in PAO sequential polymer usage, staged maintenance-decay and glycolysis-TCA pathway shifts. More importantly, we further calibrated and verified the model by leveraging the power of single-cell Raman microspectroscopy technology that enabled cellular-level quantification of intracellular dynamics under various conditions [8,41,56]. The model was first calibrated using a previously published 8-day anaerobic starvation testing in PAO-enriched (85% as PAO) EBPR batch reactor [33]. Then the calibrated model was validated using an independent 72-hour continuous anaerobic incubation batch test with sludge from a full-scale S2EBPR system. The model outperformed the previous model in predicting the experimentally observed trends of intracellular polymer biomass content under anaerobic conditions and was proven to be more effective in simulating PAO/GAO maintenance behavior under those extended anaerobic conditions than conventional models. The proposed mechanism can be incorporated into industrial EBPR models to more accurately reveal the overall EBPR performance and PAO/GAO competitive dynamics as observed in S2EBPR systems.

METHODOLOGY

Agent-based EBPR model structure

An agent-based EBPR model (named as iEBPR) was developed based on the model (named as iAlgae) developed by Bucci et al. (2012) [56]. In this study, three population groups are included, namely PAOs, GAOs and OHOs (ordinary heterotrophic organisms, accounting for all non-PAO/GAO biomasses). The agent-based approach splits each biomass category in 10,000 agents

(representing cell groups with phenotypic heterogeneity) with randomly seeded polymer contents and kinetic parameters.

The metabolic framework and structure of iAlgae were developed based on the International Water Association's Activated Sludge Model v2 (ASM2) that includes Accumulibacter-PAOs and OHOs [34]. A third organism type, namely Competibacter-like GAO, is added to the new model based on the current understanding of the main cell activities of GAOs including anaerobic VFA-uptake, PHA synthesis and aerobic biomass growth PHA-degradation and glycogen-accumulation [2,24,31]. At this stage, the iAlgae uses only acetate to represent all VFA species without differentiating various VFAs such as propionate etc. Similarly, PHB was chosen to represent PHA as in similar modelling study [38]. As we focused on PAO-GAO competition under extended anaerobic condition, denitrifiers, nitrifiers and other anoxic-related metabolisms are not included in this modeled. The hydrolysis and fermentation of inert organic matter was considered not bottlenecking the rbCOD generation and was modeled as instant transformation to the final VFA product. All modeled processes for Accumulibacter-PAOs, Competibacter-GAOs and OHOs are shown in **Table S1-3** with Gujer matrices.

Agent-level energy derivation for cell maintenance and decay with polymer-availability dependence

Similar to previous studies [37,38], sequential polymer usage and staged cell maintenance-decay was incorporated into the model however at agent-level. This process replaces the first-order decay calculation in ASM2. Specifically, this was modeled in two steps below.

Cell maintenance and sequential polymer usage. Each PAO and GAO agent possesses a parameter called targeted cell-maintenance rate, denoted as m^{ATP}, expressed in mol-ATP/(C-mol biomass.hr). The unit was further converted to fit the unit specifications in our model (mg polyP-P and mg glycogen-COD) based on known stoichiometry and yield coefficients reported in the previous studies [2,4,31,33]. Its proto-value was experimentally determined in previous studies [2,7,31]. In agent-based modeling, the value may vary based between agents to emulate the metabolic heterogeneity between cells and phenotypes. Each PAO and GAO agent will attempt to fulfill their own cell-maintenance target according on their local intracellular polymer availability. Specifically, GAOs will generate ATP via the previously proposed stoichiometry [2,31] when glycogen is available. For PAO cells, the same glycogen-based stoichiometry was used [33] as well as the stoichiometry of ATP production from polyP cleavage [4]. In addition, extra mechanism must be introduced to allocate the contributions from both glycogen and polyP based on the agent phenotype of preferences. For polyP-preferred agents, this was calculated as

$$r_{polyP} = M_{polyP} m^{ATP}$$

$$r_{glycogen} = M_{glycogen}\left(m^{ATP} - r_{polyP}\right),$$

while for glycogen-preferred agents, this was calculated as

$$r_{glycogen} = M_{glycogen} m^{ATP}$$

$$r_{polyP} = M_{polyP}\left(m^{ATP} - r_{glycogen}\right)$$

instead. Where: r_{polyP} and $r_{glycogen}$ are the real-time ATP generation rate from the respective polymer; m^{ATP} is the target cell-maintenance rate; M_{polyP} and $M_{glycogen}$ are Monod functions scaling the production rate based on the availability of the respective polymer. It is important to note that this calculation strategy can be easily extended to calculation with more than two polymers in sequential preferences. This approach simulates the observed sequential polymer usage in various studies [29,32,33]. Unlike other models reported in the literature where the sequence of polymer usages is pre-chosen [37,38], we set the polymer preference order as an adjustable parameter to simulate the PAO metabolic versatility and observations with inconsistent prioritization [32,33].

Sequential and linked cell maintenance and decay. Previous EBPR models considered the cell decay as an intrinsic process at a constant specific rate i.e., first-order decay. A number of studies have showed evidence of accelerated biomass decay after depletion of their intracellular polymers, implying a linkage between these two processes [29,33]. To simulate this linkage, we first calculated the combined ATP production from all involved polymers in cell maintenance, then compared it with the target cell-maintenance rate (denoted as m^{ATP}) [26]. If the production is short from the target, the proportion of the shortage was used as a switching function to scale the actual biomass decay rate, namely,

$$b_r = b_{max}\left(1 - \frac{r^{ATP}}{m^{ATP}}\right),$$

where: b_r is the actual specific decay rate; b_{max} is the maximum specific decay rate; r^{ATP} is the combined ATP production from cell maintenance processes. The decayed biomass then proportionally regenerates as VFA (rbCOD) based on the empirical PAO/GAO biomass formula

$CH_{1.93}O_{0.53}N_{0.2}$ [2]. This calculation states a "maintenance precedes decay" mechanism that PAO and GAO biomasses are able to suffer no biomass decay when they have ample polymer for cell maintenance. In other words, the cell maintenance was hypothesized as a "survival" strategy for PAO and GAO cells under anaerobic conditions [38].

Glycolysis and TCA cycle pathway switching

As discussed previously, current knowledge suggests that PAOs can use both glycolysis and TCA cycle to generate the reducing power needed in PHA synthesis. The major difference between glycolysis-oriented and TCA-oriented metabolism (including various TCA-cycle operation patterns) is glycogen dependency [45,47]. Namely, PHA synthesis solely supported by TCA cycle will remain operatable after glycogen depletion [25,45]. Dominant use, or a combined employment at various degrees of these two pathways have been evidenced and discussed [20,27,28,43–48,57]. In this study, we simplify the metabolic network to two principal stoichiometry models, namely sole glycolysis (Mino model) [28,57] and full TCA cycle (Comeau-Wentzel model) [27,43], which are both well established, and widely adopted in EBPR modeling applications. To simulate the various degrees of deployment of these two pathways, the final stoichiometry was calculated as their weighted mixture, where the weights of respective pathway was calculated from the availability of respective polymers. This is considered as a common approach which was also used by previous studies in both stoichiometric analysis [45,47] and modelling [37,38]. Therefore, the change of polymer availability during simulation will also change the weight ratio between pathways, simulating the polymer-dependent pathway shift. However, this calculation implies that PAOs much rely on polyP in PHA synthesis and disallows them shifting to GAO-like metabolism; though it is not necessarily true in reality [25,58]. In addition, to account for the PAO phenotypes that may strictly

require glycogen in PHA synthesis [28,50], we also included a second type of PAO agents that cannot switch to TCA-oriented metabolism when glycogen is depleted. This multi-phenotype feature within a single biomass category is exclusive to agent-based modelling.

Agent pool initialization and discrete-time simulation

All agents were generated by randomizing the cellular states and kinetic traits via individual seeding distributions, which can be calibrated with observation datasets revealing in-species heterogeneities. Only the cellular biomass, polymer storage, rates and affinity-related traits are randomized; stoichiometric coefficients are considered as pre-determined constants as they can be theoretically determined or empirically justified. The number of agents is an important parameter in agent-based modeling. A larger agent pool trends to have generated traits statistically better approximate the pre-defined seeding distributions, however, will proportionally increase the computational load. We found that using 1,000-10,000 agents per biomass was a good compromise. In addition, we used discrete-time simulation approach with all agents updated synchronously at each simulated time step.

Model Calibration

Simulation of the PAO and GAO competition under extended anaerobic conditions via the modified agent-based EBPR model (iEBPR) was first calibrated with an independent set of data retrieved from a previous 8-day anaerobic starvation study in a lab-scale Accumulibacter-enriched (reported abundance of ~85%) EBPR system [33]. The initial content of glycogen and PHA was acquired from the published data with the polyP estimated by assuming a full cleavage and release at the end of the experimental period. Anaerobic kinetic parameters of PAOs and GAOs are calibrated. Gradient descent technique is used as automated calibration method. For detail, the

geometric mean of root mean square errors (RMSEs) calculated from predicted and observed temporal profiles of PHA, glycogen, orthophosphate and MLVSS was used as the loss function. The gradient descent algorithm hence could start from an arbitrary initial parameter set then iteratively adjust those parameter values in the direction where the loss function reduces the fastest, until hitting a local minimum. The global optimum was attempted by repeating the above process for 10,000 times; then the final parameter set corresponds to the least loss was selected as the calibration result. Yield coefficients used the values from previous studies and ASM2 model defaults with unit conversions if necessary [2,7,59]. **Table S4-6** shows the final parameter set for PAOs and OHOs respectively, and unit conversions are shown in **Note S7**.

Comparison of model results with cellular-level experimental observations via single-cell Raman microspectroscopy

Previous studied proposed single-cell Raman spectroscopy (SCRS) to be a promising technology in estimating the glycogen, PHA and polyP in individual cells, to further reveal the polymer distributions at both cellular and population levels. [41,60–62]. This phenotypic survey data is comparable with the polymer distribution predicted by agent-based modelling [56].

SCRS dataset acquisition. An SCRS dataset was first acquired for each individually sludge sample based on the method detailed in previous studies [1,8,41]. Briefly, 1 mL of MLSS was washed twice with 0.9% (w/v) NaCl solution and homogenized by passing in and out of a 26-gauge needle and syringe for at least 20 times to obtain uniform distribution of cells, as described previously. Then 6-8 drops of the disrupted sample were spread and dried on aluminum-coated slides (EMF Corp., Ithaca, US). After that, the slide was dipped into ice-cold Milli-Q water several times to remove

277 salt particles, and dried by filtered nitrogen gas. For each sample, Raman spectra for at least 40
278 single cells were acquired using a multiline confocal Raman spectrometer (LabRam HR Evolution,
279 Horiba Jobin Yvon, Kyoto, Japan) configured with a 532 nm Nd:YAG laser and a 600 gr/mm
280 grating. A 100× long working distance objective with a numerical aperture (NA) of 0.9 and a
281 working distance of 0.21 mm was used to observe and collect Raman signal from single cells. The
282 acquisition time for each individual spectrum was 20 seconds per cell and the laser power was set
283 to 10%. Spectra were collected with scan from 400 cm^{-1} to 1800 cm^{-1}.

284 ***SCRS data processing.*** Raman spectra processing and polymer relative abundance calculation
285 were detailed by Gu et al. (2018)[1]. All Raman spectra were processed using cosmic spike removal,
286 smoothing, background subtraction and baseline correction using LabSpec 6 software (Horiba
287 Jobin Yvon, Kyoto, Japan). Quality control was conducted by excluding the spectra showing
288 unexpected signals (damaged) or low SNR, or lack of major characteristic peaks from bacterial
289 components such as phenylalanine (~1002 cm^{-1}) and amide I (~1657 cm^{-1}). The candidate PAO
290 and GAO populations were quantified based on the different combinations of intracellular
291 polymeric inclusions, including poly-P (band at 690-700 cm^{-1} for P-O-P vibrations and band at
292 1168-1177 cm^{-1} for PO_2^- stretching band), PHAs (bands at ~434 cm^{-1},~839 cm^{-1}, and ~1723 cm^{-1}),
293 and glycogen (bands at ~480 cm^{-1},~852 cm^{-1}, and ~938 cm^{-1}), as described previously [62]. The
294 relative content of poly-P, PHAs, and glycogen in each candidate PAO and GAO cell were
295 evaluated based on the intensity of the bands at 1168-1177 cm^{-1}, ~1723 cm^{-1}, and ~480 cm^{-1},
296 respectively (normalized against the intensity of the amide I band). The polymer distribution in
297 PAO and GAO biomass was then estimated based on the polymer relative abundances within PAO
298 and GAO candidate cells collected in each sample respectively.

RESULTS AND DISCUSSION

Model calibration with batch testing results

The model was calibrated against the temporal profile of orthophosphate and residual ammonia concentration, intracellular glycogen and PHA storage (Figure 1). The ammonia concentration was calculated from the modeled biomass decay in the same method proposed by Lu et al. (2007) [33]. Figure 1 shows the comparison of the experimental data with the predicted orthoP, ammonia, glycogen and PHA temporal profiles by the improved model and previous agent-based model iEBPR (without the staged maintenance-decay and sequential polymer utilization for cell maintenance). The improved iEBPR model performed quantitatively better than the previous iAlgea model (Table 1). Particularly, note that the revised model reflects the "S-shape" of the orthoP profile indicating a first acceleration and then deceleration of polyP degradation. While the previous model predicted a deviated profile without this acceleration. The glycogen profiles are predicted with similar trend from both models; while only the improved model predicted the increase in polyP-origin ATP production from Day 1-3 resulted from the sequential polymer utilization that shifted from glycogen-dependent to poly-P dominant. Based on these experimental observations, the 8-day anaerobic starvation could be divided into four phases: Day 0-1: Glycogen degradation phase signatured by fast glycogen reservoir depletion within the first day, accompanied by corresponding PHA formation; Day 1-2: Continuous glycogen degradation but with a slower rate until the end of Day 2; the PHA formation rate was also lowered concurrently. The glycogen content was still above detection limit after this stage, but no significant change was observed afterwards. Meanwhile, there was minimal decay of biomass (indicated by releasing residual ammonia); Day 2-4: PolyP degradation phase accompanied with increasing residual

321 orthoP concentration and slowly increasing residual ammonia implying no significant cell decay;
322 Day 4-8: Decelerating releasing rate of phosphate indicated the degradation of polyP was slowing
323 down, which was accompanied with detectable increase in the residual ammonia signifying
324 accelerated cell biomass decay.

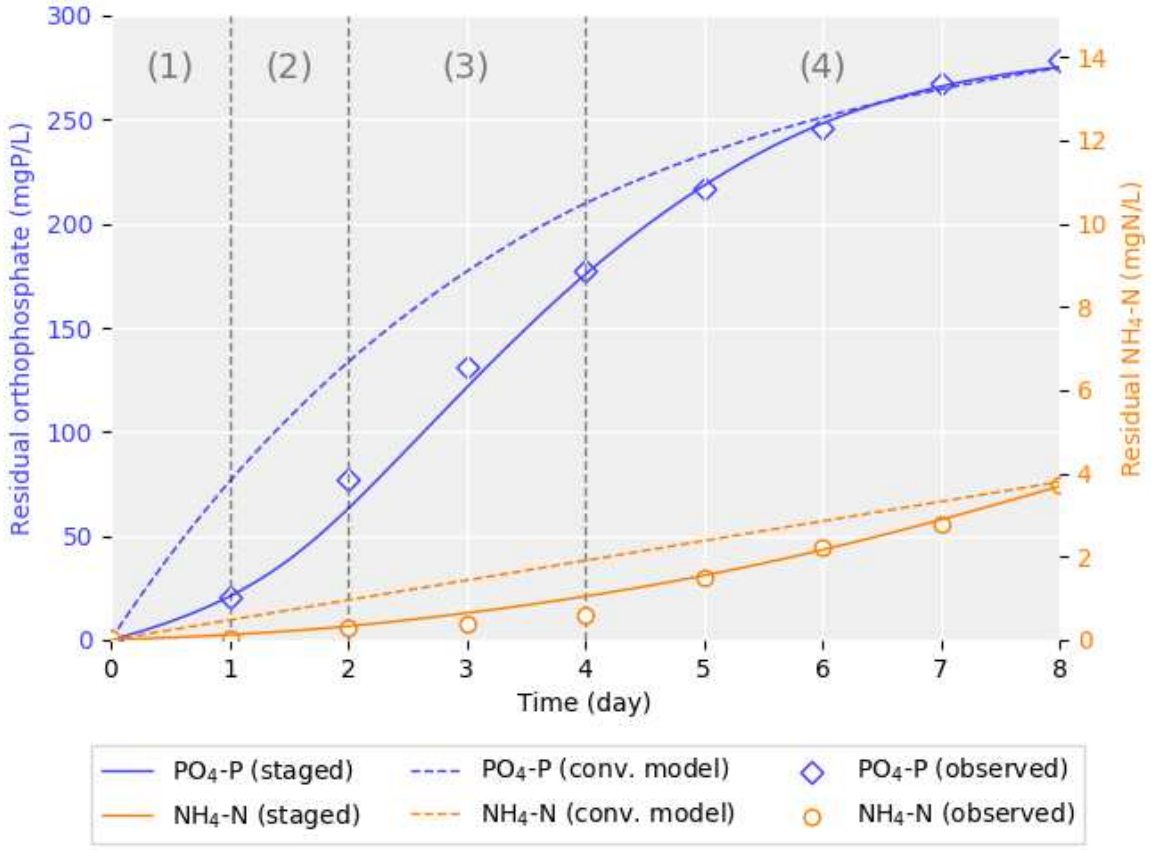

325

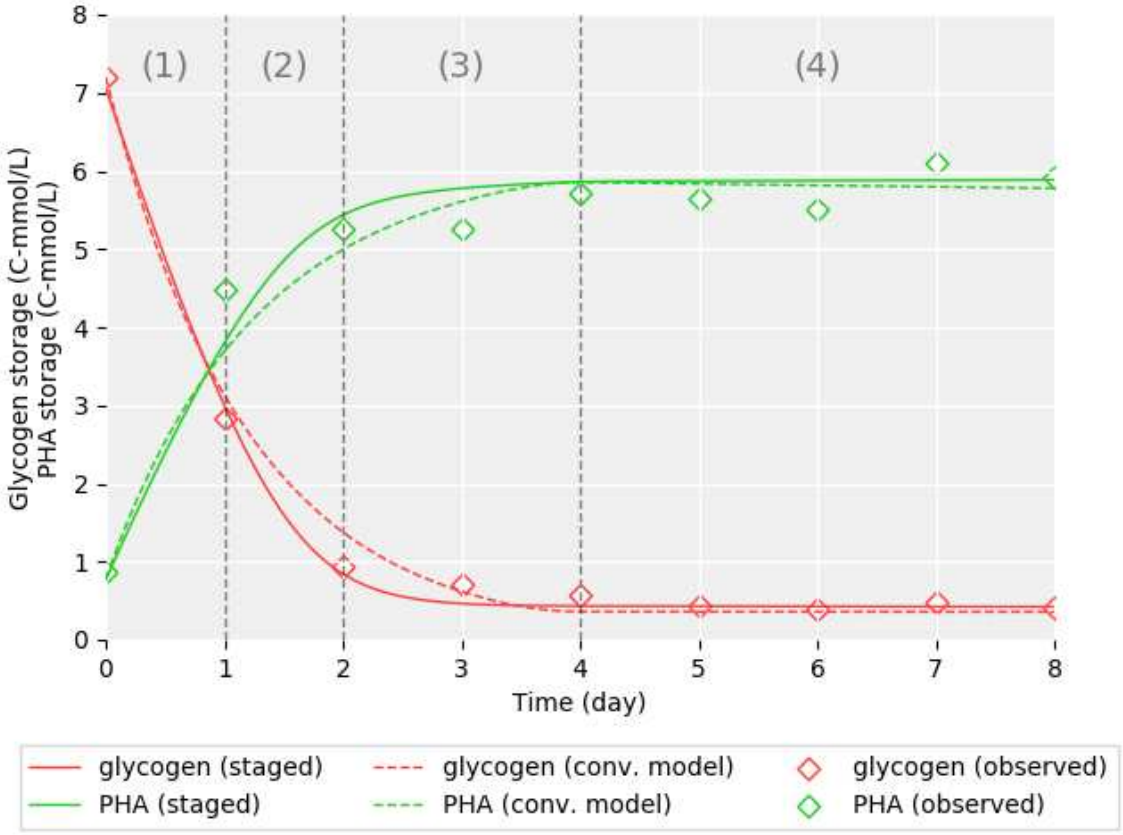

Figure 1. Model calibration by comparing the simulations results via the iEBPR model against the temporal experimentally measured profiles of PO_4-P, ammonia, intracellular glycogen and PHA in an acetate-fed lab-scale EBPR system with approximately 85% Accumulibacter-PAOs during an 8-day anaerobic starvation batch test (Lu et al. (2007)). Top shows the residual orthophosphate and ammonia-nitrogen profiles, and the bottom shows intracellular glycogen and PHA. Results were also compared with the simulation results from the previous iAlgae model that uses first-order polymer decay. Number (1)-(4) indicate the four differential stages observed during the batch test: (1) rapid glycogen degradation; (2) transit stage with decreasing glycogen depletion rate and increasing polyP hydrolysis rate; (3) polyP degradation with glycogen being depleted; and (4) polyP depleting stage with on-set of significant cell decay (indicated by the increased release of residual ammonia).

Notably, the calibrated PAO cell maintenance rate was 2.1×10^{-3} mol ATP/(C-mol VSS·hr), which resided in the range shown in Table 1. The model calibration suggested that only a very small or portion of PAOs (< 1%) can utilize TCA cycle. This agreed with the results found in original experiment where no significant PHA formation was observed after glycogen depletion [33].

Table 1. Modelling accuracy (RMSE) comparison between iEBPR and iAlgae. Observation data acquired from an 8-day anaerobic starvation test of an acetate-fed PAO-enriched (about 85% as PAOs) lab-scale sludge by Lu et al. (2007).

Model	RMSE			
	PO_4-P mgP/L	NH_4^+-N mgN/L	PHA C-mol/L	Glycogen C-mol/L
iEBPR (Improved with staged maintenance-decay, sequential anaerobic maintenance polymer usage and glycolysis-TCA pathway switching, this study)	5.98	0.18	0.34	0.12
iAlgae-ASM2[34,56]	33.0	1.08	0.34	0.19

Improved accuracy in predicting PAOs' competitive advantage

Comparing to the Lu et al. (2007)'s original experimental data, both the improved iEBPR and the conventional iAlgea models predicted a high-rate glycogen utilization in the first stage day, while, only the improved model that incorporated staged maintenance and decay was able to predict the accelerated polyP degradation upon the depletion of glycogen as observed in the stage 2 and 3. This suggested that Accumulibacter-like PAOs biomass seemed to prefer the utilization of glycogen over poly-P as energy source when both are available as they are consumed first and fulfilled the theoretical cell-maintenance ATP requirements. This was accompanied by the transition from glycogen-oriented towards a polyP-oriented cell maintenance. Figure 2 shows the calculated distribution of ATP production originated from the glycogen versus those from polyP.

Note that the previous model (iAlgae) that uses the first-order decay to approximate cell maintenance failed to reflect the observed transition from dominantly glycogen-dependent ATP

358 production to a stage with accelerated polyP utilization upon the depletion of glycogen (Figure 1
359 and Figure 2). The overestimation of PAOs' polyP consumption under anaerobic conditions within
360 the first 24 hrs (more relevant to the anaerobic condition in full-scale EBPR systems) hence may
361 underestimate the PAOs' competition advantage under anaerobic conditions. This overestimated
362 polyP cleavage caused the traditional model to over-predict about 56 mgP/L P release than the
363 observation at the end of Day 2 Figure 1 (top). The incorporation of the staged-maintenance and
364 decay with sequential polymer utilization better predicted PAOs biomass decay kinetics under
365 anaerobic conditions comparing to conventional model.

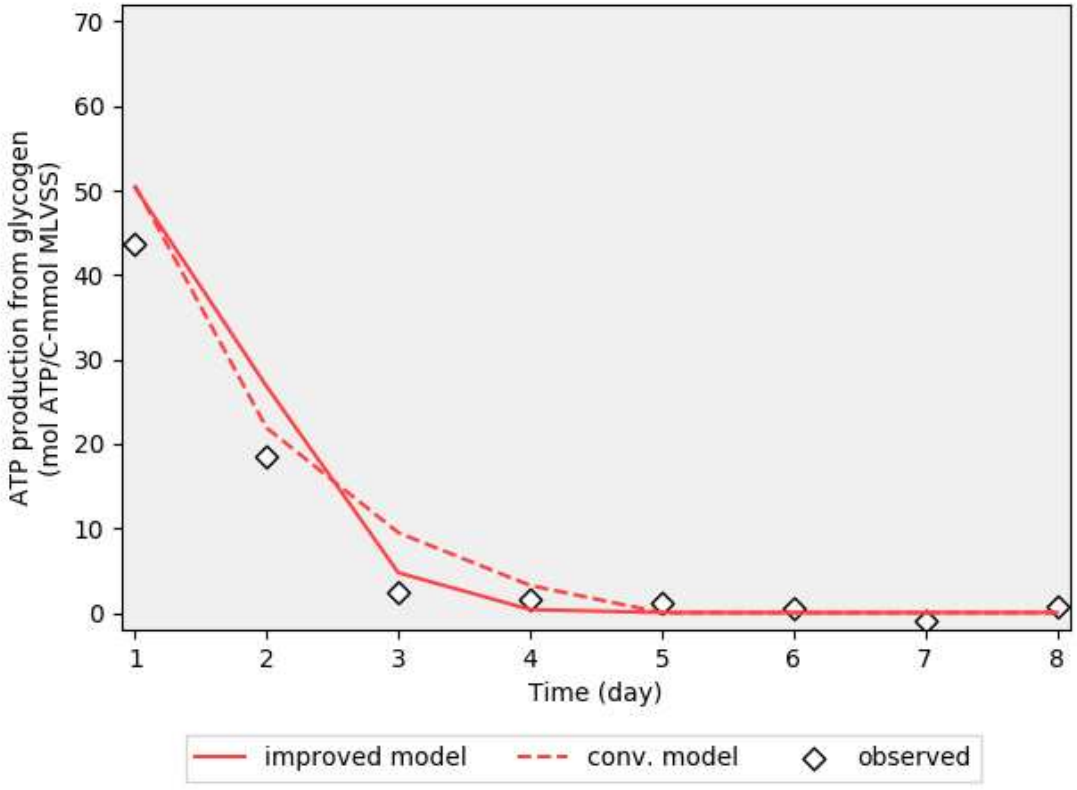

366

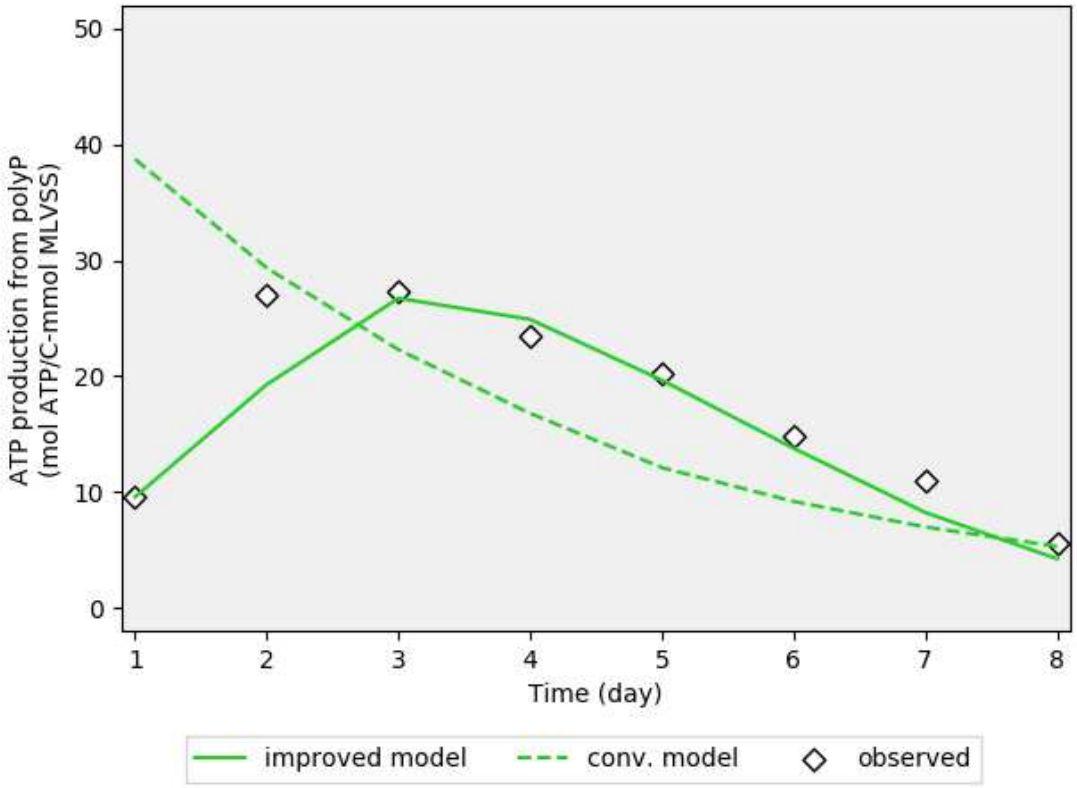

367

368 Figure 2. Comprison of model predictions and experimental observations of glycogen-contributed (top) and
369 polyP-contributed (bottom) ATP during an 8-day anaerobic starvation testing with acetate-fed lab-scale
370 EBPR system containing about 85% as Accumulibacter-PAOs (used as calibration dataset) by Lu et al.
371 (2007). The improved model (this study) is designed with sequential anaerobic maintenance polymer usage,
372 staged maintenance-decay and glycolysis-TCA pathway shift; iAlgae uses the same first-order decay as
373 ASM2 [34,56].

374 The staged maintenance-decay mechanism also predicts a different PAO biomass decay kinetics
375 from those by the traditional first-order model. An accelerating release of ammonia nitrogen was
376 observed in the experiments which accompanied with the deceleration of polyP release at the end
377 of Day 4. This indicates the PAO cells approached the depletion of both intracellular polymers and
378 started decay, as the nitrogen-containing substance began to lysis from dying cells as ammonia
379 [33,63]. The improved model captured the ammonia release acceleration by using the staged
380 maintenance-decay mechanism (Figure 1 top). The calibrated PAOs biomass decay rate was

381 0.007/d, being close to the reported value as 0.006/d as reported in original experiment. To predict
382 the same amount of biomass decay using the traditional constant first-order lysis mechanism, the
383 decay rate had to be calibrated to 0.0028/d (the dash line of NH_4^+-N in Figure 1 (top)), which is
384 53% less than the reported value. This inaccurate approximation of biomass decay when using
385 traditional model may potentially lead to either overestimating PAO biomass loss before their
386 polymer depletion or underestimating the PAOs' biomass loss after. This effect can have much
387 more impact on simulating processes with extended anaerobic incubation HRT such as in S2EBPR
388 system, therefore it is crucial to incorporate this mechanism in order to improve the modeling
389 performance of a variety of S2EBPR systems.

390 **Case study: Simulating PAO and GAO competition under prolonged anaerobic incubation**
391 **using Full-scale S2EBPR biomass**

392 **Model prediction at bulk level**

393 The calibrated model was used to simulate an independent anaerobic incubation batch testing
394 similar to the conditions in side-stream reactor in S2EBPR systems [64]. The testing sludge was
395 sampled from the side-stream fermentation reactor (SSR configuration) of South Cary Water
396 Reclamation Facility (Apex, North Carolina) as described by Nicholas et al. (2018) and Onnis-
397 Hayden et al. (2018) [9,64]. It was estimated to contain 6.9% biovolume as Accumulibacter-PAOs
398 and 1.1% as known GAOs by fluoresces in-situ hybridization (FISH) [64]. The batch test was
399 conducted as a 72-hour anaerobic incubation without external VFA feeding, and the residual
400 orthophosphate, residual VFA, MLSS glycogen and PHA were monitored and measured at 0, 6,
401 12, 18, 24, 36 and 72 hours after the beginning of this incubation. The model was fitted to these

402 temporal profiles with adjustment on initial status and biomass-composition-related parameters,
403 including initial polymer contents, biomass concentration of all three species and the fraction of
404 TCA-cycle-enabled agents in PAO species. In addition, OHOs' biomass decay rate was also
405 adjusted to the experimentally identified value. All other kinetic and stoichiometric parameters
406 were set identical to the lab-scale sludge calibration results, no more kinetic calibrations were
407 conducted. GAOs' kinetic and stoichiometric parameters were set identical to PAOs' except the
408 yield ratio of PHA to VFA uptake, since GAOs lack polyP and rely on glycogen to provide both
409 ATP and reducing power in this process [2,7].

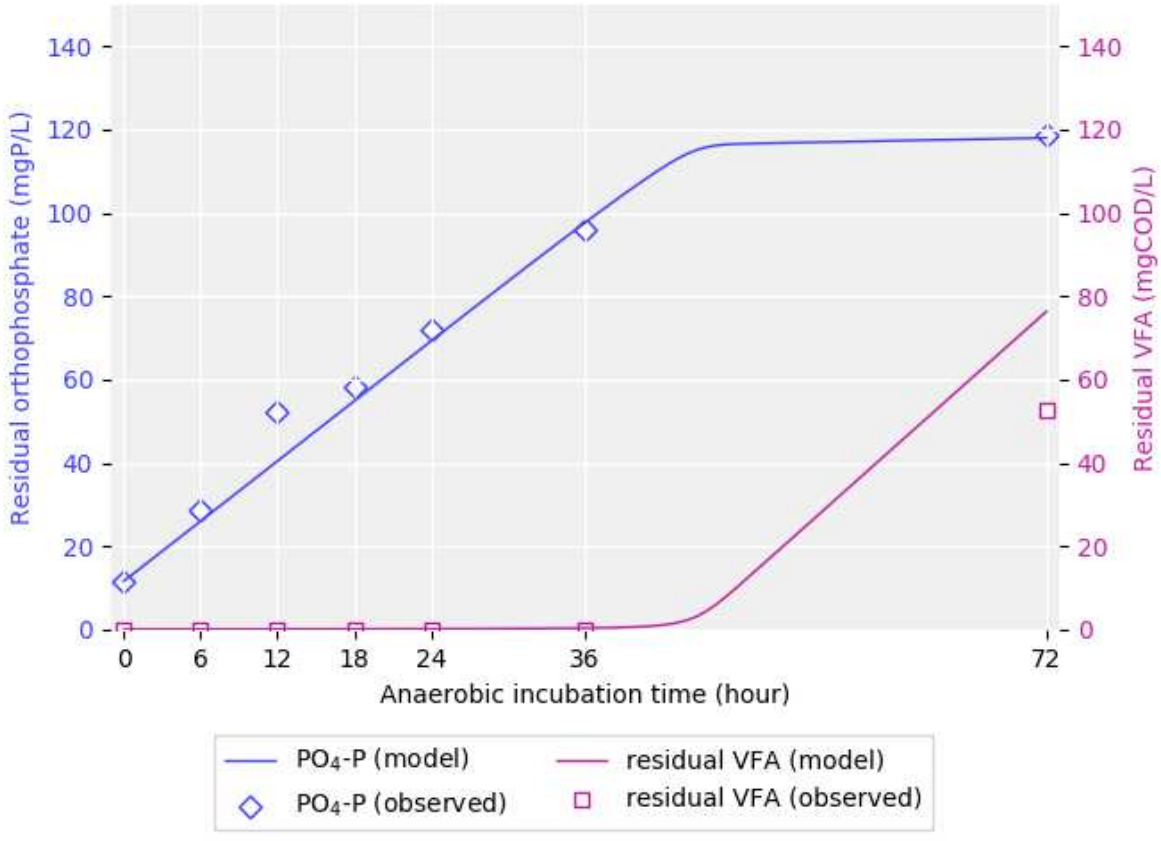

410

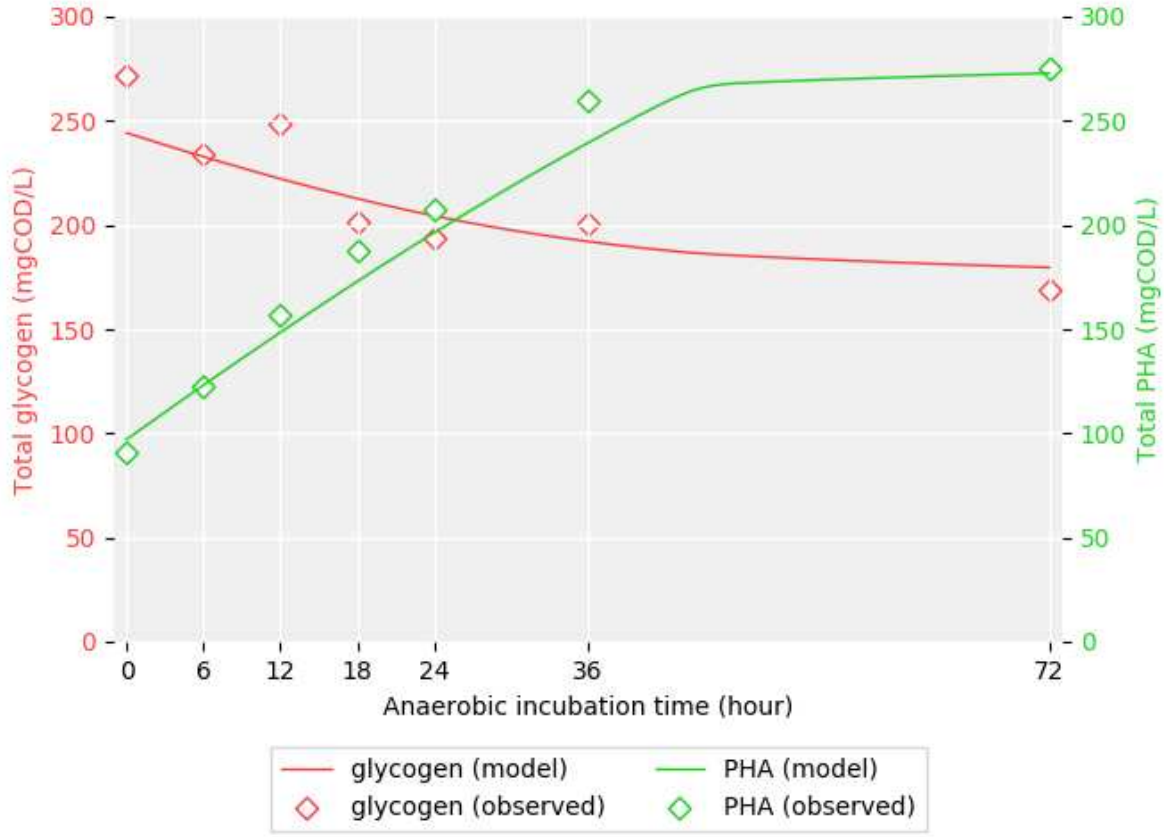

411

412 Figure 3. Comparison of experimental measurements with Simulated temporal trends of residual orthoP,
413 intracellular PHA and glycogen in a 72-hour anaerobic incubation batch test using sludge sampled from
414 full-scale S2EBPR system (SSR configuration, South Cary WRF, Apex, NC) estimated to contain 6.9% as
415 Accumulibacter-PAO, 1.1% as GAOs (by FISH, biovolume), using the improved model iEBPR that
416 incorporates sequential polymer utilization in cell maintenance, staged maintenance-decay and glycolysis-
417 TCA pathway shift. Top: residual orthophosphate and residual VFA; Bottom: MLSS glycogen and PHA.

418 Figure 3 shows the comparison of the observed measurements with the predicted temporal profiles
419 of residual PO_4-P, residual VFA, total MLSS PHA and glycogen during the anaerobic batch
420 testing. The OHO decay rate was calculated to be 0.0076/d based on the VFA requirement to fit
421 the observed stoichiometry of P release, glycogen consumed and PHA formation, since in this
422 model the hydrolysis and fermentation process is integrated into biomass decay. The simulated

423 residual PO_4-P, MLSS glycogen and PHA agreed well with observed data with RMSEs of
424 4.9mgP/L, 16.5mgCOD/L and 11.15 mgCOD/L respectively; the RMSE of residual VFA was
425 8.9mgCOD/L and about 22mgCOD/L VFA was overestimated by the model at 72 hours. The
426 model predicted a transitioning at around 45 hours from high-rate active P release with significant
427 PHA synthesis phase to a second phase with slower increase in both PHA and residual P.
428 Calculated yield ratio of the active P release to PHA formation from 36-72 hours was 1.77 mol-
429 P/C-mol PHA, which is higher than the typical range 0.36-0.77 mol-P/C-mol PHA for A/O
430 enriched sludge [4,30,36,47] and 0.78-1.22 mol-P/C-mol PHA for S2EBPR sludge [20]. This implies an
431 excessive source was contributing to the PO_4-P release which was not related to VFA uptake and
432 PHA formation, potentially being cell maintenance.

433 **Model prediction at cellular and population level**

434 However, investigate detailed polymer transformation at this bulk level is limited due to the lack
435 of resolution of real-time polymer distribution at population and cellular levels that better reflect
436 the competition between PAOs and GAOs , which may result in different metabolic patterns co-
437 exist according to the actual polymer storage in individual cells. To further validate the proposed
438 mechanism of polymer-dependent and staged maintenance and decay, SCRS was employed to
439 measure and reveal the intracellular polymer dynamics in PAOs and GAOs that ultimately dictates
440 their competition, and they were compared with the agent-based model results. The initial
441 distributions of PAOs' and GAOs' intracellular polymers namely polyP and glycogen in PAOs
442 and glycogen in GAOs, were adjusted manually after their means were determined in the previous
443 bulk-level step following the previous protocol [56]. Their temporal trends were represented by
444 snapshotting the modeled residue polymers across PAO/GAO species at 0, 6, 12, 24 36 and 72

445 hours, and were compared to the experimentally acquired distributions by SCRS at the same time
446 points. [41,60,61]. As shown in Figure 4, the model accurately predicted the measurements at cellular
447 and population levels, proving that the model mechanisms to be effective in modeling highly
448 resolved PAO/GAO intracellular polymer metabolisms.

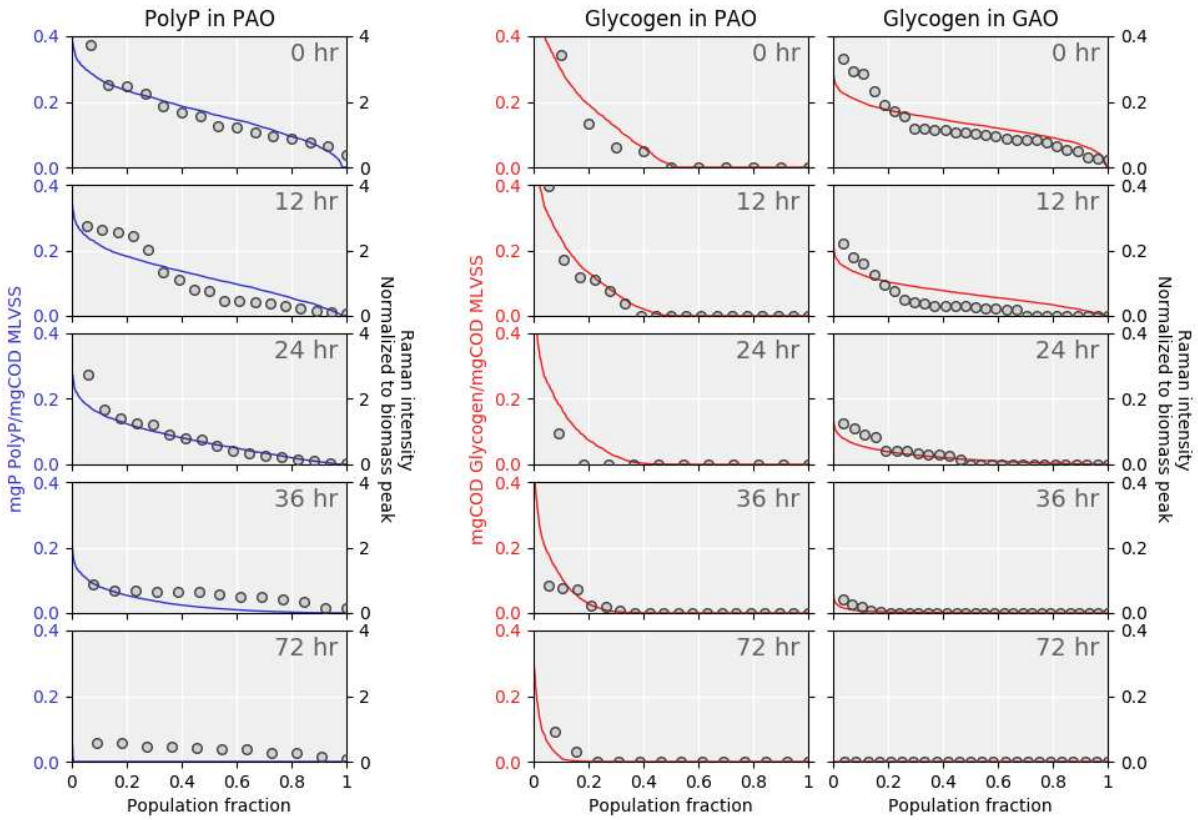

449

450 Figure 4. PAO polyP, glycogen and GAO glycogen in-species distribution by agent-based modeling (lines)
451 and the actual distribution acquired by Raman single-cell microspectrascopy (dots) during a 72-hranaerobic
452 incubation batch test (this study) with sludge sampled from full-scale S2EBPR system (SSR configuration,
453 South Cary WRF, Apex, NC).

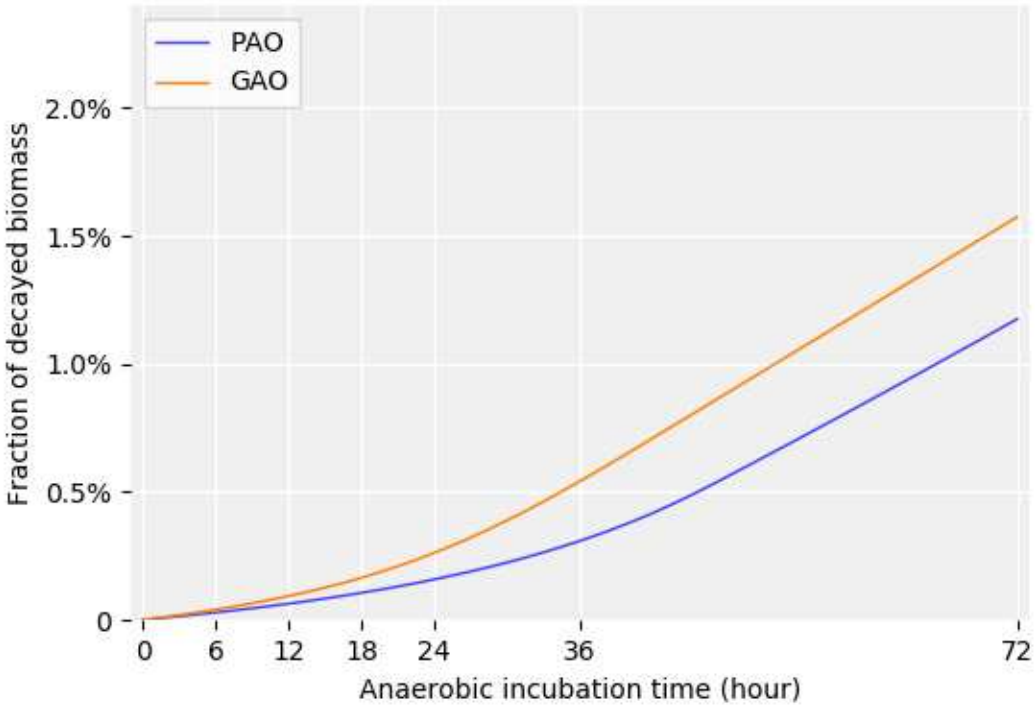

454

455 Figure 5. iEBPR predicted PAO and GAO decay based on sequential polymer utilization in cell
456 maintenance and staged maintenance-decay mechanism of a 72-hour anaerobic incubation batch test using
457 sludge sampled from full-scale S2EBPR system (SSR configuration, South Cary WRF, Apex, NC)
458 estimated to contain 6.9% as Accumulibacter-PAO, 1.1% as GAOs (by FISH, biovolume). GAOs were
459 speculated to have more cumulative biomass decay due to their earlier depletion of intracellular polymers.
460 Agent-based modeling predicted slower and less PAOs decay than GAOs.

461 ***PAO-GAO competition.*** The SCRS dataset showed a clear 2-phase glycogen depletion trend in
462 GAO cells: (1) an active utilization phase before 36 hours; (2) nearly depleted to a full depletion
463 within 36-72 hours. The glycogen in PAOs showed a similar decreasing trend but a portion of the
464 PAO cells contained detectable amount of glycogen up to 72 hours. In contrary to the faster
465 depletion, GAO cells were estimated to contain higher initial glycogen contents. The mean
466 available glycogen content in GAO cells was estimated to be 0.126 mgCOD/mgMLVSS COD,
467 while was 0.098 mgCOD/mgMLVSS COD in PAO cells. This difference agreed with previous

468 studies suggesting that GAOs has a higher capability of glycogen storages [2,28,29,57]. The faster
469 depletion indicated that the GAOs have higher overall glycogen utilization rate than PAOs under
470 such conditions. The model identified this difference as an indication that the two independent
471 sources, polyP and glycogen, potentially provide larger amount of energy (ATP) anaerobically.
472 Hence PAOs may gain competitive advantage over GAOs for persisting a longer period of
473 maintenance under extended anaerobic conditions, and potentially start decay later and slower in
474 the first 36 hours of incubation (Figure 4, Figure 5). This differential decay rates in PAOs and
475 GAOs would likely contribute to the PAO's competitive advantage over GAOs under prolonged
476 anaerobic conditions. As a result, the staged maintenance-decay model predicted GAOs had 33%
477 more cumulative biomass decayed (1.6%) than PAOs (1.2%) during the 72-hr incubation (Figure
478 5). Meanwhile, the model predicted a complete depletion of polyP at 72 hours, which is consistent
479 with the relatively consistent residue polyP level in PAOs as revealed by the SCRS. This implies
480 a background amount of polyP potentially from non-PAO cells or "inert" polyP portion which is
481 not releasable [35].

482 ***Glycolysis-TCA pathway switch.*** SCRS data revealed that only about half of observed PAO
483 population contained glycogen at the beginning of this anaerobic incubation (Figure 4). Some of
484 the Accumulibacter-PAOs could have accumulated glycogen below SCRS detection limit, or there
485 were non-Accumulibacter-PAOs that had different metabolisms, for example, Tetrasphaera [65,66].
486 A comprehensive model for these non-Accumulibacter-PAOs is still under active exploration. In
487 addition, current knowledge assumes that PHA is always the final product of glycogen degradation
488 in Accumulibacter-PAOs' anaerobic metabolism [45,47]. Therefore assuming all PAOs being
489 Accumulibacter-PAOs may potentially lead to an over-prediction of overall PHA formation since
490 PHA is not synthesized by Tetrasphaera [65]. Under these assumptions, the model suggested that

491 almost all PAO cells in this case study can use TCA cycles to support PHA synthesis, and the
492 employment of TCA cycle was predicted to be at greater extent of involvement comparing to the
493 glycolysis-based metabolism. This was supported by the observed consistent, continuous P release
494 and PHA formation independent to the decreasing availability of glycogen. Detailed calculations
495 on the agent-based simulation results showed that PAOs had accumulated 0.20 C-mol VFA/C-mol
496 VSS by the end of 72 hours, which was significantly higher than GAOs VFA uptake, 0.61 C-mol
497 VFA/C-mol VSS. Using the stoichiometry of 0.22 mol NAD(P)H/C-mol VFA (TCA cycle) [43] and
498 0.33 mol NAD(P)H/C-mol VFA (using glycogen) [45], it is calculated that 59% of total reducing
499 power consumed in PAOs' PHA synthesis was provided from TCA cycle during the 72hr
500 incubation. This further indicates that under extended anaerobic phases as in S2EBPR, the PAOs
501 may gain competitive advantage over GAOs due to the possession of multiple intracellular
502 polymers and the adaptive switching of the anaerobic metabolic pathways.

503 The iEBPR agent-based model that incorporates the sequential polymer usage, staged
504 maintenance-decay processes and glycolysis-TCA pathway shift was developed, which was
505 calibrated and validated using both bulk batch test experimental data and high-resolution cellular
506 and population-level measurements enabled by SCRS. These newly proposed model modifications
507 are expected to improve the simulation accuracy on S2EBPR systems, particularly SSR (side-
508 stream RAS fermentation) and SSRC (SSR with carbon addition) configurations where a longer
509 anaerobic S2EBPR SRT may lead to the manifestation of more complicated PAO/GAO
510 competition metabolisms that differ from those in play in conventional EBPR systems (i.e. A2O
511 configuration). The model revealed that under extended anaerobic phases as in S2EBPR, the PAOs
512 may gain competitive advantage over GAOs due to the possession of multiple intracellular
513 polymers and the adaptive switching of the anaerobic metabolic pathways that consequently lead

514 to longer maintenance period prior to the later and slower decay in PAOs compared with shorter
515 maintenance period before the earlier and faster decay in GAOs. The iEBPR model can be applied
516 to facilitate and optimize the design and operations of S2EBPR for more reliable nutrient removal
517 and recovery from wastewater.

518 **REFERENCES**

519 (1) Gu, A. Z.; Tooker, N. B.; Onnis-Hayden, A.; Wang, D.; Li, G.; Srinivasan, V.; Takács, I.
520 *Investigation of the Mechanisms for Optimization and Design of a Side-Stream EBPR*
521 *Process as a Sustainable Approach for Achieving Stable and Efficient Phosphorus*
522 *Removal*.; WE&RF, 2018.
523 (2) Zeng, R. J.; van Loosdrecht, M.; Yuan, Z.; Keller, J. Metabolic Model for Glycogen-
524 accumulating Organisms in Anaerobic/Aerobic Activated Sludge Systems. *Biotechnol.*
525 *Bioeng.* **2003**, *81* (1), 92–105.
526 (3) Oehmen, A.; Zeng, R. J.; Saunders, A. M.; Blackall, L. L.; Keller, J.; Yuan, Z. Anaerobic
527 and Aerobic Metabolism of Glycogen-Accumulating Organisms Selected with Propionate
528 as the Sole Carbon Source. *Microbiology* **2006**, *152* (9), 2767–2778.
529 (4) Smolders, G.; Van der Meij, J.; Van Loosdrecht, M.; Heijnen, J. Model of the Anaerobic
530 Metabolism of the Biological Phosphorus Removal Process: Stoichiometry and PH
531 Influence. *Biotechnol. Bioeng.* **1994**, *43* (6), 461–470.
532 (5) Gu, A. Z.; Saunders, A.; Neethling, J.; Stensel, H.; Blackall, L. Functionally Relevant
533 Microorganisms to Enhanced Biological Phosphorus Removal Performance at Full-Scale
534 Wastewater Treatment Plants in the United States. *Water Environ. Res.* **2008**, *80* (8), 688–
535 698.
536 (6) Neethling, J.; Bakke, B.; Benisch, M.; Gu, A.; Stephens, H.; Stensel, H. D.; Moore, R.
537 *Factors Influencing the Reliability of Enhanced Biological Phosphorus Removal*; Water
538 Environment Research Foundation, 2006.
539 (7) Lopez-Vazquez, C. M.; Oehmen, A.; Hooijmans, C. M.; Brdjanovic, D.; Gijzen, H. J.; Yuan,
540 Z.; van Loosdrecht, M. C. Modeling the PAO–GAO Competition: Effects of Carbon Source,
541 PH and Temperature. *Water Res.* **2009**, *43* (2), 450–462.
542 (8) Majed, N.; Gu, A. Z. Insights into the Metabolic Pathways and Diversity of Functionally
543 Relevant Populations in Enhanced Biological Phosphorus Removal Processes Using Raman
544 Microscopy. *Proc. Water Environ. Fed.* **2011**, *2011* (11), 4824–4832.
545 (9) Onnis-Hayden, A.; Tooker, N.; Srinivasan, V.; Gu, A. Survey of Plants Operating in Side-
546 Stream EBPR Mode and Comparison with Conventional: Process Stability, Kinetics and
547 Microbial Population (in Review).
548 (10) Nielsen, P. H.; McIlroy, S. J.; Albertsen, M.; Nierychlo, M. Re-Evaluating the Microbiology
549 of the Enhanced Biological Phosphorus Removal Process. *Curr. Opin. Biotechnol.* **2019**,
550 *57*, 111–118.
551 (11) Wang, D.; Tooker, N. B.; Srinivasan, V.; Li, G.; Fernandez, L. A.; Schauer, P.; Menniti, A.;
552 Maher, C.; Bott, C. B.; Dombrowski, P.; Barnard, J. L.; Onnis-Hayden, A.; Gu, A. Z. Side-
553 Stream Enhanced Biological Phosphorus Removal (S2EBPR) Process Improves System

554 Performance - A Full-Scale Comparative Study. *Water Res.* **2019**, *167*, 115109.
555 https://doi.org/10.1016/j.watres.2019.115109.
556 (12) Barnard, J.; Abraham, K. Key Features of Successful BNR Operation. *Water Sci. Technol.*
557 **2006**, *53* (12), 1–9.
558 (13) Barnard, J.; Houweling, D.; Analla, H.; Steichen, M. Fermentation of Mixed Liquor for
559 Phosphorus Removal. *Proc. Water Environ. Fed.* **2010**, *2010* (18), 59–71.
560 (14) Stevens, G.; Ellsworth, A.; Wyman, M.; Lambrecht, A. BNR Process Using RAS Anaerobic
561 Zone. *Proc. Water Environ. Fed.* **2015**, *2015* (3), 1–3.
562 (15) Stroud, R.; Martin, C. South Cary Water Reclamation Facility's Nutrient Removal
563 Modifications and Reduction Success, Town of Cary, North Carolina. *Proc. Water Environ.*
564 *Fed.* **2001**, *2001* (14), 337–345.
565 (16) Copp, J. B.; Belk, I.; Vale, P. Operational Control of a RAS Fermentation Process for
566 Enhancing Biological Phosphorus Removal. *Proc. Water Environ. Fed.* **2012**, *2012* (9),
567 6056–6068.
568 (17) Vale, P.; Barnard, J.; Thomas, D.; Dold, P. RAS Fermentation to Enhance Biological
569 Phosphorus Removal. In *Proceedings of the WEFTEC Conference*; 2008.
570 (18) Vollertsen, J.; Petersen, G.; Borregaard, V. R. Hydrolysis and Fermentation of Activated
571 Sludge to Enhance Biological Phosphorus Removal. *Water Sci. Technol.* **2006**, *53* (12), 55–
572 64.
573 (19) Srinivasan, V. N.; Li, G.; Wang, D.; Tooker, N. B.; Dai, Z.; Onnis-Hayden, A.; Pinto, A.;
574 Gu, A. Z. Oligotyping and Genome-Resolved Metagenomics Reveal Distinct Candidatus
575 Accumulibacter Communities in Full-Scale Side-Stream versus Conventional Enhanced
576 Biological Phosphorus Removal (EBPR) Configurations. *bioRxiv* **2019**, 596692.
577 (20) Lanham, A. B.; Oehmen, A.; Saunders, A. M.; Carvalho, G.; Nielsen, P. H.; Reis, M. A.
578 Metabolic Versatility in Full-Scale Wastewater Treatment Plants Performing Enhanced
579 Biological Phosphorus Removal. *Water Res.* **2013**, *47* (19), 7032–7041.
580 (21) Mielczarek, A. T.; Nguyen, H. T. T.; Nielsen, J. L.; Nielsen, P. H. Population Dynamics of
581 Bacteria Involved in Enhanced Biological Phosphorus Removal in Danish Wastewater
582 Treatment Plants. *Water Res.* **2013**, *47* (4), 1529–1544.
583 (22) Stokholm-Bjerregaard, M.; McIlroy, S. J.; Nierychlo, M.; Karst, S. M.; Albertsen, M.;
584 Nielsen, P. H. A Critical Assessment of the Microorganisms Proposed to Be Important to
585 Enhanced Biological Phosphorus Removal in Full-Scale Wastewater Treatment Systems.
586 *Front. Microbiol.* **2017**, *8*, 718.
587 (23) Dunlap, P.; Martin, K.; Stevens, G.; Tooker, N.; Barnard, J.; Gu, A.; Takacs, I.; Shaw, A.;
588 Onnis-Hayden, A.; Li, Y. Rethinking EBPR: What Do You Do When the Model Will Not
589 Fit Real-World Evidence? 5th IWA. In *WEF Wastewater Treatment Modeling Seminar,*
590 *Annecy, France*; 2016; pp 39–62.
591 (24) Houweling, D.; Comeau, Y.; Takács, I.; Dold, P. Uncertainty and Variability in Enhanced
592 Biological Phosphorus Removal (EBPR) Stoichiometry: Consequences for Process
593 Modelling and Optimization. *Water Sci. Technol.* **2010**, *61* (7), 1793–1800.
594 (25) da Silva, L. G.; Gamez, K. O.; Gomes, J. C.; Akkermans, K.; Welles, L.; Abbas, B.; van
595 Loosdrecht, M. C.; Wahl, S. A. Revealing Metabolic Flexibility of Candidatus
596 Accumulibacter Phosphatis through Redox Cofactor Analysis and Metabolic Network
597 Modeling. *bioRxiv* **2018**, 458331.
598 (26) Li, G.; Tooker, N. B.; Wang, D.; Srinivasan, V.; Barnard, J. L.; Schauer, P.; Takács, I.;
599 Onnis-Hayden, A.; Gu, A. Z. Application of Agent-Based Modeling to Reveal Competition

between PAOs and GAOs in Side-Stream EBPR (S2EBPR) Systems. *Proc. Water Environ. Fed.* **2018**, *2018* (5), 269–274.

(27) Wentzel, M.; Dold, P.; Ekama, G.; Marais, G. Enhanced Polyphosphate Organism Cultures in Activated Sludge Systems. Part III: Kinetic Model. *Water A* **1989**, *15* (2), 89–102.

(28) Mino, T.; Van Loosdrecht, M.; Heijnen, J. Microbiology and Biochemistry of the Enhanced Biological Phosphate Removal Process. *Water Res.* **1998**, *32* (11), 3193–3207.

(29) Vargas, M.; Yuan, Z.; Pijuan, M. Effect of Long-Term Starvation Conditions on Polyphosphate-and Glycogen-Accumulating Organisms. *Bioresour. Technol.* **2013**, *127*, 126–131.

(30) Filipe, C. D.; Daigger, G. T.; Grady, C. Effects of PH on the Rates of Aerobic Metabolism of Phosphate-Accumulating and Glycogen-Accumulating Organisms. *Water Environ. Res.* **2001**, *73* (2), 213–222.

(31) Filipe, C. D.; Daigger, G. T.; Grady, C. A Metabolic Model for Acetate Uptake under Anaerobic Conditions by Glycogen Accumulating Organisms: Stoichiometry, Kinetics, and the Effect of PH. *Biotechnol. Bioeng.* **2001**, *76* (1), 17–31.

(32) Lopez, C.; Pons, M.; Morgenroth, E. Endogenous Processes during Long-Term Starvation in Activated Sludge Performing Enhanced Biological Phosphorus Removal. *Water Res.* **2006**, *40* (8), 1519–1530.

(33) Lu, H.; Keller, J.; Yuan, Z. Endogenous Metabolism of Candidatus Accumulibacter Phosphatis under Various Starvation Conditions. *Water Res.* **2007**, *41* (20), 4646–4656.

(34) Henze, M.; Harremoes, P.; la Cour Jansen, J.; Arvin, E. *Wastewater Treatment: Biological and Chemical Processes*; Springer Science & Business Media, 2001.

(35) Barker, P.; Dold, P. General Model for Biological Nutrient Removal Activated-Sludge Systems: Model Presentation. *Water Environ. Res.* **1997**, *69* (5), 969–984.

(36) Hu, Z.; Wentzel, M.; Ekama, G. A General Kinetic Model for Biological Nutrient Removal Activated Sludge Systems: Model Development. *Biotechnol. Bioeng.* **2007**, *98* (6), 1242–1258.

(37) Lanham, A. B.; Oehmen, A.; Saunders, A. M.; Carvalho, G.; Nielsen, P. H.; Reis, M. A. Metabolic Modelling of Full-Scale Enhanced Biological Phosphorus Removal Sludge. *Water Res.* **2014**, *66*, 283–295.

(38) Santos, J. M.; Rieger, L.; Lanham, A. B.; Carvalheira, M.; Reis, M. A.; Oehmen, A. A Novel Metabolic-ASM Model for Full-Scale Biological Nutrient Removal Systems. *Water Res.* **2020**, *171*, 115373.

(39) Hauduc, H.; Rieger, L.; Oehmen, A.; Van Loosdrecht, M.; Comeau, Y.; Héduit, A.; Vanrolleghem, P.; Gillot, S. Critical Review of Activated Sludge Modeling: State of Process Knowledge, Modeling Concepts, and Limitations. *Biotechnol. Bioeng.* **2013**, *110* (1), 24–46.

(40) Li, G.; Tooker, N. B.; Wang, D.; Srinivasan, V.; Onnis-Hayden, A.; Barnard, J. L.; Russel, A.; Bott, C. B.; Schauer, P.; Dombrowski, P.; Shaw, A.; Stinson, B.; Stevens, G.; Dunlap, P.; Phillips, H.; Analla, H.; Lambrecht, A.; McQuarrie, J.; Takács, I.; Gu, A. Z. Modeling Side-Stream Enhanced Biological Phosphorus Removal (S2EBPR) Systems: Insights from Versatile Anaerobic Pathways. *Proc. Water Environ. Fed.* **2020**.

(41) Majed, N.; Matthäus, C.; Diem, M.; Gu, A. Z. Evaluation of Intracellular Polyphosphate Dynamics in Enhanced Biological Phosphorus Removal Process Using Raman Microscopy. *Environ. Sci. Technol.* **2009**, *43* (14), 5436–5442.

(42) Mino, T.; Arun, V.; Tsuzuki, Y.; Matsuo, T. Effect of Phosphorus Accumulation on Acetate Metabolism in the Biological Phosphorus Removal Process. In *Biological phosphate removal from wastewaters*; Elsevier, 1987; pp 27–38.

(43) Comeau, Y.; Hall, K.; Hancock, R.; Oldham, W. Biochemical Model for Enhanced Biological Phosphorus Removal. *Water Res.* **1986**, *20* (12), 1511–1521.

(44) Maurer, M.; Gujer, W.; Hany, R.; Bachmann, S. Intracellular Carbon Flow in Phosphorus Accumulating Organisms from Activated Sludge Systems. *Water Res.* **1997**, *31* (4), 907–917.

(45) Zhou, Y.; Pijuan, M.; Zeng, R. J.; Yuan, Z. Involvement of the TCA Cycle in the Anaerobic Metabolism of Polyphosphate Accumulating Organisms (PAOs). *Water Res.* **2009**, *43* (5), 1330–1340.

(46) Pereira, H.; Lemos, P. C.; Reis, M. A.; Crespo, J. P.; Carrondo, M. J.; Santos, H. Model for Carbon Metabolism in Biological Phosphorus Removal Processes Based on in Vivo13C-NMR Labelling Experiments. *Water Res.* **1996**, *30* (9), 2128–2138.

(47) Yagci, N.; Artan, N.; Çokgör, E. U.; Randall, C. W.; Orhon, D. Metabolic Model for Acetate Uptake by a Mixed Culture of Phosphate-and Glycogen-Accumulating Organisms under Anaerobic Conditions. *Biotechnol. Bioeng.* **2003**, *84* (3), 359–373.

(48) Pijuan, M.; Oehmen, A.; Baeza, J. A.; Casas, C.; Yuan, Z. Characterizing the Biochemical Activity of Full-Scale Enhanced Biological Phosphorus Removal Systems: A Comparison with Metabolic Models. *Biotechnol. Bioeng.* **2008**, *99* (1), 170–179.

(49) Brdjanovic, D.; van Loosdrecht, M. C.; Hooijmans, C. M.; Mino, T.; Alaerts, G. J.; Heijnen, J. J. Bioassay for Glycogen Determination in Biological Phosphorus Removal Systems. *Water Sci. Technol.* **1998**, *37* (4–5), 541–547.

(50) Hesselmann, R.; Von Rummell, R.; Resnick, S. M.; Hany, R.; Zehnder, A. Anaerobic Metabolism of Bacteria Performing Enhanced Biological Phosphate Removal. *Water Res.* **2000**, *34* (14), 3487–3494.

(51) He, S.; McMahon, K. D. 'Candidatus Accumulibacter'Gene Expression in Response to Dynamic EBPR Conditions. *ISME J.* **2011**, *5* (2), 329.

(52) Wilmes, P.; Wexler, M.; Bond, P. L. Metaproteomics Provides Functional Insight into Activated Sludge Wastewater Treatment. *PLoS One* **2008**, *3* (3), e1778.

(53) Schuler, A. J.; Jenkins, D. Enhanced Biological Phosphorus Removal from Wastewater by Biomass with Different Phosphorus Contents, Part III: Anaerobic Sources of Reducing Equivalents. *Water Environ. Res.* **2003**, *75* (6), 512–522.

(54) Brdjanovic, D.; Van Loosdrecht, M.; Hooijmans, C.; Mino, T.; Alaerts, G.; Heijnen, J. Effect of Polyphosphate Limitation on the Anaerobic Metabolism of Phosphorus-Accumulating Microorganisms. *Appl. Microbiol. Biotechnol.* **1998**, *50* (2), 273–276.

(55) Martín, H. G.; Ivanova, N.; Kunin, V.; Warnecke, F.; Barry, K. W.; McHardy, A. C.; Yeates, C.; He, S.; Salamov, A. A.; Szeto, E.; others. Metagenomic Analysis of Two Enhanced Biological Phosphorus Removal (EBPR) Sludge Communities. *Nat. Biotechnol.* **2006**, *24* (10), 1263.

(56) Bucci, V.; Majed, N.; Hellweger, F. L.; Gu, A. Z. Heterogeneity of Intracellular Polymer Storage States in Enhanced Biological Phosphorus Removal (EBPR)–Observation and Modeling. *Environ. Sci. Technol.* **2012**, *46* (6), 3244–3252.

(57) Smolders, G.; Klop, J.; Van Loosdrecht, M.; Heijnen, J. A Metabolic Model of the Biological Phosphorus Removal Process: I. Effect of the Sludge Retention Time. *Biotechnol. Bioeng.* **1995**, *48* (3), 222–233.

(58) Acevedo, B.; Oehmen, A.; Carvalho, G.; Seco, A.; Borrás, L.; Barat, R. Metabolic Shift of Polyphosphate-Accumulating Organisms with Different Levels of Polyphosphate Storage. *Water Res.* **2012**, *46* (6), 1889–1900. https://doi.org/10.1016/j.watres.2012.01.003.

(59) Smolders, G.; Van der Meij, J.; Van Loosdrecht, M.; Heijnen, J. Stoichiometric Model of the Aerobic Metabolism of the Biological Phosphorus Removal Process. *Biotechnol. Bioeng.* **1994**, *44* (7), 837–848.

(60) Majed, N.; Gu, A. Z. Application of Raman Microscopy for Simultaneous and Quantitative Evaluation of Multiple Intracellular Polymers Dynamics Functionally Relevant to Enhanced Biological Phosphorus Removal Processes. *Environ. Sci. Technol.* **2010**, *44* (22), 8601–8608.

(61) Li, Y.; Cope, H. A.; Rahman, S. M.; Li, G.; Nielsen, P. H.; Elfick, A.; Gu, A. Z. Toward Better Understanding of EBPR Systems via Linking Raman-Based Phenotypic Profiling with Phylogenetic Diversity. *Environ. Sci. Technol.* **2018**, *52* (15), 8596–8606.

(62) Majed, N.; Gu, A. Z. Phenotypic Dynamics in Polyphosphate and Glycogen Accumulating Organisms in Response to Varying Influent C/P Ratios in EBPR Systems. *Sci. Total Environ.* **2020**, *743*, 140603.

(63) Gujer, W. *The Activated Sludge Model No. 2: Biological Phosphorus Removal: Proceedings IAWQ Specialised Seminar: Modelling and Control of Activated Sludge Processes, 22.-24. August 1994, Copenhagen*; IAWQ, 1994.

(64) Tooker, N.; Li, G.; Srinivasan, V.; Onnis-Hayden, A.; Gu, A. Elucidating the Mechanisms of Side-Stream Enhanced Biological Phosphorus Removal (in Review).

(65) Kristiansen, R.; Nguyen, H. T. T.; Saunders, A. M.; Nielsen, J. L.; Wimmer, R.; Le, V. Q.; McIlroy, S. J.; Petrovski, S.; Seviour, R. J.; Calteau, A.; others. A Metabolic Model for Members of the Genus Tetrasphaera Involved in Enhanced Biological Phosphorus Removal. *ISME J.* **2013**, *7* (3), 543.

(66) Fernando, E. Y.; McIlroy, S. J.; Nierychlo, M.; Herbst, F.-A.; Petriglieri, F.; Schmid, M. C.; Wagner, M.; Nielsen, J. L.; Nielsen, P. H. Resolving the Individual Contribution of Key Microbial Populations to Enhanced Biological Phosphorus Removal with Raman–FISH. *ISME J.* **2019**, 1.